JBC Papers in Press. Published on March 5, 2013 as Manuscript M113.458133
The latest version is at http://www.jbc.org/cgi/doi/10.1074/jbc.M113.458133

Structural sensitivity of a prokaryotic pentameric ligand-gated ion channel to its membrane environment*

Jonathan M. Labriola[1], Akash Pandhare[2], Michaela Jansen[3], Michael P. Blanton[2], Pierre-Jean Corringer[4], and John E. Baenziger[1]

[1]From the Department of Biochemistry, Microbiology, and Immunology
University of Ottawa, Ottawa ON, K1H 8M5, Canada

[2]Department of Pharmacology and Neuroscience and the Center for Membrane Protein Research, School of Medicine, Texas Tech University Health Sciences Center, Lubbock, TX 79430

[3]Department of Cell Physiology and Molecular Biophysics and the Center for Membrane Protein Research, School of Medicine, Texas Tech University Health Sciences Center, Lubbock, TX. 79430.

[4]G5 Group of Channel-Receptors, CNRS URA 2182
Pasteur Institute, F75015, Paris, France

*Running title: *Lipid sensitivity of a prokaryotic pLGIC*

[1]To whom correspondence should be addressed: John E. Baenziger, Department of Biochemistry, Microbiology, and Immunology, University of Ottawa, 451 Smyth Rd. Ottawa, ON, K1H 8M5, Canada, Tel.: (613) 562-5800 x8222; Fax.: (613) 562-5440; E-mail: John.Baenziger@uottawa.ca.

Keywords: prokaryotic pentameric ligand-gated ion channels, membrane sensitivity, structure, function

Background: The lipid sensitivity of the prokaryotic pentameric ligand-gated ion channel (pLGIC), GLIC, is poorly characterized.
Results: GLIC is more thermally stable and does not exhibit the same propensity to adopt an uncoupled conformation as the *Torpedo* nAChR.
Conclusions: GLIC is less sensitive to its surrounding membrane environment.
Significance: The GLIC and nAChR structures suggest molecular features governing the lipid sensitivity of pLGICs.

SUMMARY

Although the activity of the nicotinic acetylcholine receptor (nAChR) is exquisitely sensitive to its membrane environment, the underlying mechanisms remain poorly defined. The homologous prokaryotic pentameric ligand gated ion channel, GLIC, represents an excellent model for probing the molecular basis of nAChR sensitivity due to its high structural homology, ease of expression, and amenability to crystallographic analysis. We show here that membrane-reconstituted GLIC exhibits structural and biophysical properties similar to those of the membrane-reconstituted nAChR, although GLIC is substantially more thermally stable. GLIC, however, does not possess the same exquisite lipid sensitivity. In particular, GLIC does not exhibit the same propensity to adopt an uncoupled conformation where agonist binding is uncoupled from channel gating. Structural comparisons provide insight into the chemical features that may predispose the nAChR to the formation of an uncoupled state.

Cys-loop receptors mediate rapid chemical communication between cells in the nervous system by opening a transmembrane ion channel across the synaptic membrane in response to neurotransmitter binding. Channel opening leads to the flow of either cations or anions down their electrochemical gradient into the cell, resulting in either an excitatory or an

inhibitory response, respectively. Cys-loop receptors play a central role in brain function, are implicated in a variety of neurological disorders, and are the targets of both endogenous and exogenous modulators (1-5).

Early attempts at purifying and reconstituting the prototypic Cys-loop receptor, the *Torpedo* nicotinic acetylcholine receptor (nAChR)[5], in lipid bilayers revealed the importance of lipids in Cys-loop receptor function (6). In the presence of both cholesterol and anionic lipids, the nAChR is stabilized predominantly in an activatable resting conformation (7-10). In their absence, the nAChR adopts an "uncoupled" conformation, where agonist binding fails to elicit channel gating (11). Understanding the mechanisms by which lipids influence the coupling of binding and gating remains central to understanding lipid-nAChR interactions. Uncoupled nAChRs may also have broader significance in that neuronal nAChRs that are functionally uncoupled have been observed in heterologous expression systems and may play a role in the physiological response to nicotine (see (12)). Unfortunately, detailed insight into the mechanisms of lipid-dependent uncoupling remains elusive (11,13). A major bottleneck is the inability to reliably express large quantities of Cys-loop receptors with site-directed mutations designed to test potential models of lipid-nAChR interactions.

Several prokaryotic pentameric ligand-gated ion channels (pLGICs) homologous to the eukaryotic Cys-loop receptors have recently been identified, and crystal structures of two of these, GLIC and ELIC, solved at high resolution (14-17). Prokaryotic pLGICs provide an opportunity for probing the mechanisms of Cys-loop receptor-lipid interactions at a molecular level owing to their high structural homology (Fig. 1), their ease of expression in bacterial systems, and their amenability to crystallographic analysis. While a recent study suggested that cholesterol depletion may influence GLIC gating kinetics (18), the broader effects of lipids on prokaryotic pLGIC structure and function remain to be studied. In fact, a reliable protocol for reconstituting prokaryotic pLGICs in membranes at lipid to protein ratios that are amenable to spectroscopic studies, particularly in the context of probing the electrophysiologically silent uncoupled state, has yet to be developed.

Here, we compare the structural and biophysical properties of membrane-reconstituted GLIC to those of its highly lipid-sensitive eukaryotic homolog, the *Torpedo* nAChR. These comparisons were performed in membranes that both support GLIC/nAChR function and those that promote formation of the uncoupled nAChR. Our results suggest that while the gating properties of GLIC are sensitive to its lipid environment, GLIC does not possess the exquisite lipid-sensitivity of its eukaryotic homolog. In particular, GLIC does not exhibit the same propensity to adopt an uncoupled conformation where agonist binding is uncoupled from channel gating. Structural comparisons provide insight into the chemical features that may predispose Cys-loop receptors to the formation of an uncoupled state

EXPERIMENTAL PROCEDURES

Materials. Soybean asolectin (L-α-phosphatidylcholine, type II-S), sodium cholate, carbamylcholine (Carb), and amantadine were from Sigma (St. Louis, MO). *E. coli* polar lipid extracts and 1-palmotyl-2-oleoyl-*sn*-glycero-3-phosphocholine were from Avanti (Alabaster, AL). *Torpedo californica* electroplaque organ was from Aquatic Research Consultants (San Pedro, CA). Dodecylmaltoside (DDM) was from Affymetrix (Santa Clara, CA). [^{125}I]-α-Bungarotoxin (107 Ci/mmol) was obtained from PerkinElmer Life Sciences (Boston, MA). Non-radioactive α-Bungarotoxin was from Biotium, Inc (Hayward, CA)

GLIC expression and purification. GLIC was expressed in the C43 strain of *E. coli* transformed with a pET-20b(+) vector containing the DNA sequence for the maltose binding protein fused to the N-terminus of GLIC through a thrombin-sensitive peptide linker (14). Briefly, 2 litre cultures of the transformed C43 cells were grown in 2YT media containing 50ug/mL ampicillin at 37˚C to an OD_{600} of ~1.2 a.u, and the cultures induced overnight at 30˚C with 100μM IPTG. Cells were harvested, resuspended in Buffer A (250mM NaCl, 25mM Tris, pH7.2) in the presence of Roche Complete™ antiprotease tablets (Branford, CT),

and lysed with an Avestin Emulsiflex-C5 homogenizer (Ottawa, Canada). Membrane fractions were solubilised in 1% DDM in Buffer A and the GLIC fusion protein bound to an amylose affinity resin. After treatment with plasminogen-free thrombin from Calbiochem (Gibbstown, NJ), GLIC was eluted in 0.02% DDM and further purified on Superpose 6 10/300 gel-filtration column (GE Healthcare; Little Chafont, UK). The highly purified GLIC was passed quickly through 1ml of amylose resin to remove small amounts of an endogenous amylose binding protein that co-elutes with GLIC from the size exclusion column.

Membrane reconstitution of GLIC. The purified GLIC in 0.02% DDM in buffer A was slowly diluted at least 1:4 with lipids solubilised in 0.625% cholate in Buffer A to give the desired final lipid-to-protein ratio, in this case 2:1 (w/w) (19,20). After gently mixing for ~30 minutes, the protein/detergent/lipid mixture was dialyzed five times at 4˚C against 2L of Buffer A leading to a turbid solution of proteoliposomes, which were harvested by ultracentrifugation at 100,000g for 2h. The pelleted membranes were re-suspended and layered onto a discontinuous sucrose-density gradient. After ultracentrifugation at 100,000g for 20h in a Beckman SW41 swinging bucket rotor, sequential 400uL aliquots were removed and assayed for both protein (BCA™ assay from Thermo-Pierce; Rockford, IL) and lipid (Phospholipid C/Choline assay from Wako Chemicals; Richmond, VA). Appropriate fractions were pooled and either dialyzed a further 5 times or subjected to several centrifugation resuspension cycles to remove sucrose.

Reconstituted nAChR membranes. nAChR purification and reconstitution was performed as described (11,21). The nAChR was solubilised from *Torpedo* electroplacques with 1% sodium cholate and purified on a bromoacetylcholine affinity column in the presence of lipid. Protein was eluted with 10 mM carbamylcholine (Carb) and then membrane reconstituted by dialysis.

Fourier transform infrared spectroscopy. Hydrogen/deuterium infrared spectra (Fig. 2a) were recorded on a Digilab (now Agilent Technologies; Santa Clara, CA) FTS40 spectrometer using a Golden-Gate™ attenuated total internal reflection accessory (SpecAc; Oprington, Kent, U.K.). 10 µl of the membrane-reconstituted GLIC (~1 mg/ml) in 2mM phosphate buffer (pH 7.0) were dried down onto the accessory under a gentle stream of N_2 gas. After collecting a 64 scan spectrum at 4 cm^{-1} resolution, 10 µl of buffer A in ^2H_2O was added and another 64 scan spectrum collected.

For the more detailed amide I band analyses (Fig. 2b) and for thermal stability measurements, the membrane reconstituted GLIC was exchanged into 2mM phosphate ^2H_2O buffer, pH 7.0 for precisely 72 hours at 4˚C and then stored at -80 ^oC until use. Approximately 125µg of GLIC was deposited on a CaF_2 window with a gentle stream of N_2 gas followed by rehydration with 8µL of Buffer A in ^2H_2O, pH 7.0. A 4000 scan spectrum was collected at 2 cm^{-1} resolution and 22.5 ^oC on a Digilab (now Agilent Technologies; Santa Clara, CA) FTS7000 spectrometer. 128 scan spectra were then acquired at 1˚C intervals from 35 ^oC – 90 ^oC with a 20 minute equilibration period between each temperature jump.

Spectra were analyzed using GRAMS/AI software (Thermo Scientific; Waltham, MA). Residual water vapor was subtracted using the method of Reid et al (22). Resolution enhancement was performed between 1900 cm^{-1} and 1300 cm^{-1} using a $\gamma = 7$ and a Bessel smoothing function set to 70%. Thermal denaturation was measured as the change in intensity at 1681 cm^{-1} and was evaluated using Graphpad Prism (La Jolla, CA) (11).

Electrophysiology. Electrophysiology was performed using a two electrode voltage clamp apparatus (OC-725C oocyte clamp; Holliston, MA) or as described elsewhere (23). Except where noted, oocytes were injected with 100ng of membrane-reconstituted GLIC or nAChR, or 6.6ng of GLIC mRNA and allowed to incubate for 1-2 days at 16˚C in ND96+ buffer (5mM HEPES, 96mM NaCl, 2mM KCl, 1mM $MgCl_2$, 1mM $CaCl_2$, and 2mM Pyruvate). Injected oocytes were placed in a RC-1Z oocyte chamber (Harvard Apparatus; Hamden, CT) containing MES buffer (140mM NaCl, 2.8mM KCl, 2mM $MgCl_2$, and 10mM MES, pH7.0). Currents through the plasma membrane in response to pH jumps were measured with the

transmembrane voltage clamped at between -20mV or -60mV. The oocytes chamber was perfused with MES buffer at a rate of ~5mL/min.

α-Bungarotoxin binding assays. Individual oocytes were incubated with 2.58 nM [^{125}I]-α-bungarotoxin for 2 h at room temperature. Oocytes were washed 3 times with 1 mL of ice-cold buffer containing 1% BSA and then binding was quantified by gamma-counting. Nonspecific binding was determined with oocytes from the same batch incubated with 5 μM non-labeled α-bungarotoxin.

RESULTS

Membrane reconstitution of GLIC. GLIC was reconstituted into membranes at a lipid-to-protein ratio of 2:1 (wt:wt), as this ratio is ideal for spectroscopic studies, such as those used previously to characterize the uncoupled nAChR (see Discussion)(11). To reconstitute into model membranes, DDM-solubilized GLIC (see Supplemental Information, Fig. S1) was diluted below the critical micellar concentration for DDM with a cholate-solubilized lipid solution, and the protein/detergent/lipid mixture dialyzed extensively to remove residual DDM and cholate. Sucrose density gradients showed that GLIC efficiently incorporates into model membranes. Neither residual DDM nor cholate could be detected in the reconstituted membranes using an infrared based assay for detergent (24). GLIC was initially reconstituted into membranes composed of either asolectin lipids (aso-GLIC) or *E. coli* polar lipid extracts (EcoLip-GLIC). These membranes were chosen because asolectin lipids (as well as defined membranes composed of PC/PA/Chol 3:1:1 (molar ratios)) stabilize the nAChR in a functional resting conformation and minimize GLIC aggregation (18), while *E. coli* polar lipid extracts likely resemble GLIC's natural lipid environment. We expected both membranes to stabilize an activatable "resting" conformation.

Structure of membrane-reconstituted GLIC. Infrared spectra of both aso-GLIC and EcoLip-GLIC gently dried from $^{1}H_2O$ buffer (to eliminate the intense overlapping vibrations of bulk water) exhibit two relatively intense protein bands, the amide I band between 1700 and 1600 cm^{-1} and the amide II band centered near 1547 cm^{-1} (Fig. 2a). The amide I band is due primarily to peptide backbone C=O stretching and is sensitive to protein secondary structure. The amide II band, due primarily to peptide backbone C-N stretching coupled to N-^{1}H bending, is also sensitive to secondary structure, but is used primarily to monitor the exchange of peptide N-^{1}H to N-^{2}H. The amide II band shifts down in frequency from 1547 cm^{-1} to near 1450 cm^{-1} in $^{2}H_2O$ - the downshifted vibration often referred to as the amide II' band.

The GLIC amide I contour observed in spectra dried from $^{1}H_2O$ exhibits a peak maximum near 1655 cm^{-1}, due to the overlapping vibrations of α-helix and loop/random secondary structures, and a prominent broad shoulder between 1640 and 1625 cm^{-1}, due primarily to the vibrations of β-sheet. The amide I band shape is similar to that observed for functional membrane-reconstituted *Torpedo* nAChRs (Fig. S2) suggesting a similar mixed α-helix/β-sheet secondary structure. The slightly increased intensity between 1640 and 1620 cm^{-1} indicates a slightly higher β-sheet content in GLIC.

The mixed α-helix/β-sheet secondary structure of the reconstituted GLIC was confirmed by recording spectra in $^{2}H_2O$ buffer, where there is no overlap of the solvent vibrations with the amide I band (Fig. 2b). The resulting amide I contour still exhibits features at frequencies characteristic of both α-helix (1655 cm^{-1}) and β-sheet (1640-1625 cm^{-1}), as shown clearly by resolution enhancement. Curve fitting (Fig. S3) suggests roughly 35% α-helix and 40% β-sheet (Fig. S3), estimates that compare well with the crystal structure (roughly 35% α-helices with >5 residues and 30% β-sheet). The slight overestimate of β-sheet content could reflect difficulties precisely defining the start and end point of each β-strand in the crystal structure. In addition, spectra of the α-helical protein myoglobin (no β-sheet) exhibit weak intensity between 1640 and 1620 cm^{-1} demonstrating that some none β-sheet structures contribute weak amide I intensity to regions of the spectra typically assigned to β-sheet (25).

Note that we recorded spectra both immediately after exposure to (Fig. 2a) and after prolonged equilibration with $^{2}H_2O$ buffer (72

hours, 4 ^{o}C) (Fig. 2b). Spectra recorded immediately after exposure exhibit changes in band shape that result from the down shifts in frequency of solvent exposed regions of the peptide backbone. Subtle down shifts in the frequencies of amide I component bands due to turn (1700-1670 cm^{-1} region, see supplemental information), loop/random and/or α-helical structures (1655 cm^{-1} down to ~1645 cm^{-1}), and β-sheet (primarily 1640 - 1620 cm^{-1} region) are detected (26). These rapid amide I band shifts are accompanied by a drop in amide II band intensity further demonstrating the rapid exchange of peptide N-^{1}H to N-^{2}H. The spectral changes are all similar to those observed immediately upon exposure of other Cys-loop receptors to $^{2}H_2O$ (Fig. S2)(27), but differ from those typically observed for proteins with different tertiary folds (26). The results emphasize the existence of a substantial population of solvent exposed secondary structures, consistent with the large solvent exposed extramembranous agonist-binding domain in GLIC (16,17).

One particularly notable feature of the GLIC spectra is that the relatively intense 1655 cm^{-1} amide I component band, which is due to the vibrations of protiated, and thus solvent shielded, α-helical and loop/random structures, is still observed in spectra recorded after prolonged exposure of GLIC to $^{2}H_2O$. This suggests the existence of a large population of exchange-resistant and likely transmembrane α-helices, as has been characterized for the nAChR (25,28). A large population of solvent shielded peptide hydrogens is also suggested by the residual amide II band intensity (Fig. 2b). The proportion of exchange-resistant peptide hydrogens in both aso-GLIC and EcoLip-GLIC is slightly higher than in aso-nAChR, although aso-GLIC exchanges to a greater extent than EcoLip-GLIC (see Discussion). The proportion of exchange resistant peptide hydrogens in aso-nAChR was estimated to be ~40%, sufficient to account for the peptide hydrogens located in the transmembrane domain (11,29). The greater proportion of exchange resistant peptide hydrogens in GLIC is likely due to the lack of an intracellular domain - the exchange-resistant transmembrane domain of GLIC makes up a greater proportion of the total protein structure (Fig. 1).

The one notable difference between the deconvolved amide I contours of GLIC and the nAChR is the existence in the latter of a more intense band centered near 1645 cm^{-1} due to downshifted and thus peptide N-^{1}H to N-^{2}H exchanged α-helical and loop/random structures. This band appears immediately after exposure of the nAChR to $^{2}H_2O$ suggesting that the affected structures are solvent exposed (28). Solvent exposed α-helical and loop/random structures exist in the intracellular domain of the nAChR. The lack of a similarly intense band centered near 1645 cm^{-1} in the GLIC spectra is consistent with the absence of an intracellular domain in GLIC.

Finally, the thermal stabilities of both aso-GLIC and EcoLip-GLIC were examined by recording infrared spectra as a function of temperature. In both cases, increasing temperature led to changes in amide I band shape characteristic of protein denaturation (Fig. S4), confirming that the reconstituted GLIC adopts a folded structure. It is noteworthy that the previously "exchange-resistant-peptide hydrogens" in the transmembrane domain of GLIC undergoes complete N-^{1}H to N-^{2}H exchange concomitant with unfolding. This behavior is similar to that observed for the nAChR, but differs from that of proteins, such as LacY, which undergoes complete N-^{1}H to N-^{2}H exchange at elevated temperatures, but prior to unfolding (20). The latter property of LacY has been attributed to a temperature induced increase in the conformational dynamics of the transmembrane domain, whereas as the transmembrane domain of GLIC may be conformationally "static" in the absence of bound agonist. The transmembrane domain of GLIC is also not expected to undergo such large conformationally transitions (16,17,30). Both aso-GLIC and EcoLip-GLIC have higher thermal stabilities of 68.8±1.5 and 73.7±1.4 ^{o}C, respectively, than that of the nAChR ~55 ^{o}C (Fig. 3, Table 1). The higher thermal stability of GLIC is consistent with its enhanced suitability for crystallization (31).

Gating properties of the membrane-reconstituted GLIC. Although reconstituted membranes at a lipid-to-protein ratio of 2:1

(wt:wt) are ideal for spectroscopic studies, they are not useful for direct measurements of channel activity using electrophysiological approaches. Instead, we indirectly probed the activity of membrane-reconstituted GLIC by injecting the reconstituted GLIC membranes into *Xenopus laevis* oocytes and then monitoring the appearance of proton activated currents across the oocyte plasma membranes using a two electrode voltage clamp apparatus (23,32).

The feasibility of the oocyte injection approach for examining the activity of membrane reconstituted pLGICs was first tested using reconstituted nAChR membranes of defined function. Carb-induced currents that decay slowly due to desensitization are observed in oocytes injected with either aso-nAChR or phosphatidyl choline/phosphatidic acid/cholesterol-nAChR (PC/PA/Chol-nAChR) showing that the functional reconstituted nAChR membranes fuse with the oocyte plasma membrane leading to the appearance of functional nAChRs on the oocyte surface (16 fmol 16 fmol binding sites/oocyte, with 0.124 ± 0.061 μA/fmol [^{125}I]-α-bungarotoxin binding sites/oocyte; Fig. 4). In contrast, weak or negligible Carb-induced currents were observed in oocytes injected with the uncoupled and non-activatable PC-nAChR, even though the reconstituted PC membranes fuse with the plasma membrane leading to the appearance of nAChR agonist sites on the surface of the oocyte (5.5 fmol [^{125}I]-α-bungarotoxin binding sites/oocyte, with 0.0034 ± 0.0006 μA current per fmol binding sites/oocyte; Fig. 4). The lack of activity of the plasma membrane incorporated PC-nAChR (~40-fold reduction in normalized current levels compared to the injected PC/PA/Chol-nAChRs) has several possible explanations. First, the lack of activity could reflect clustering of the reconstituted membranes within the oocyte plasma membrane and thus the nAChR retaining its "reconstituted membrane" lipid environment. Such clustering of the nAChR on the oocyte surface has been suggested from previous studies of oocytes injected with reconstituted nAChR membranes (32). PC-nAChR may also be locked in an uncoupled conformation because the oocyte plasma membrane lipids do not promote transitions from uncoupled to coupled conformations. Recent studies suggest that the uncoupled nAChR in long chain PC membranes can undergo ligand-induced transitions to coupled conformations (data not shown). Finally, it is possible that detergent solubilization leads to irreversible effects on nAChR structure and function. The latter seems unlikely, however, given that detergent solubilization has no deleterious effects on the nAChR reconstituted into other membranes. In addition, no detectable effects of detergent solubilization and PC reconstitution are observed on nAChR secondary structure. Regardless, these control experiments confirm that the injection of reconstituted nAChR membranes into oocytes can, in principle, be used to indirectly assess the gating activity of reconstituted nAChRs.

We next characterized the response of uninjected, mock injected (membranes alone), and GLIC mRNA injected oocytes to jumps in proton concentration. Both uninjected and mock injected oocytes exhibit weak proton-activated currents due to endogenous acid-sensitive channels (Fig. 5). These currents, however, show a roughly linear response to proton concentration at pH values down to 3.5, are insensitive to the GLIC pore-blocker, amantadine, and had maximal currents of 0.069±0.016 μA (n=4) and 0.063±0.021 μA (n=6), respectively, at the maximal utilized proton concentration (pH 3.5). In contrast, oocytes injected with GLIC RNA exhibit robust proton-activated cationic currents (Fig. S4) with relatively large maximal currents typically close to 4 μamps. A plot of whole cell currents versus proton concentration for the latter yielded a pH_{50} for activation of 4.82±0.04 (Fig. 4b), consistent with that observed previously for oocyte-expressed GLIC (14). These proton activated currents are sensitive to the pore blocker, amantadine. 150 μM amantadine blocked close to ~50% of the pH activated currents.

Oocytes injected with either aso-GLIC or EcoLip-GLIC both exhibit currents that respond to proton concentration in a dose-dependent manner. The maximal responses at pH 3.5 of 0.181±0.008 μA (n=5) and 0.157±0.014 μA (n=5), respectively, are roughly 3-fold larger than the responses observed in mock or uninjected oocytes, yet consistent in

magnitude to the Carb-induced currents observed in aso-nAChR injected oocytes. Of particular significance, these proton-induced currents were sensitive to the GLIC channel blocker, amantadine, while the endogenous acid sensitive channels in oocytes are not. These data suggest that the reconstituted GLIC in both membranes retains the ability to gate open in response to proton binding. Interestingly, the proton concentration dependence of GLIC activation is right-shifted relative to the dose response observed with mRNA-injected oocytes, suggesting weaker proton sensitivity. A weaker proton sensitivity has also been observed for GLIC reconstituted into giant unilamellar asolectin liposomes at the high lipid-to-protein ratios required for electrophysiological studies (18). The right shifted does response supports the possibility that GLIC also clusters within the oocytes plasma membrane thus maintaining its reconstituted lipid environment. The shifted does response suggests that the gating activity of GLIC is sensitive to its membrane environment.

Effects of an uncoupling lipid environment on GLIC structure and function. We next compared the structural and functional properties of aso-GLIC and EcoLip-GLIC to that of GLIC reconstituted into PC membranes (PC-GLIC). The minimal PC environment is of interest because it stabilizes the nAChR in an uncoupled conformation that binds agonist, but does not undergo agonist-induced conformational transitions. A key goal of this work was to ascertain whether GLIC exhibits the same propensity to uncouple as the nAChR in a PC bilayer.

The uncoupled PC-nAChR exhibits biophysical properties that distinguish it from the predominantly resting state aso-nAChR (Figs 2 and 3). The secondary structure sensitive amid I contour in spectra recorded from PC-nAChR are similar to that of aso-nAChR, but deconvolution reveals a downshift in amide I component band intensity from 1655 cm^{-1} to near 1645 cm^{-1}. This change in amide I band shape occurs as a result of enhanced levels of peptide N-^{1}H/N-^{2}H exchange in the uncoupled state, as opposed to a change in the global secondary structure. The enhanced peptide N-^{1}H/N-^{2}H exchange is shown by the reduced residual amide II band intensity in spectra recorded from PC-nAChR versus aso-nAChR. The absence of a change in secondary structure is shown by comparing the amide I bands of PC-nAChR and aso-nAChR at equivalent levels of peptide N-^{1}H/N-^{2}H exchange (but different exposure times to ^2H_2O). In the latter case, no significant differences in amide I contour were observed (33).

A more detailed analysis of the peptide N-^{1}H/N-^{2}H exchange kinetics of uncoupled versus resting or desensitized nAChRs shows that regions of the polypeptide backbone that are buried from solvent in the resting conformation become exposed to solvent in the uncoupled state (11). The uncoupled PC-nAChR also undergoes thermal denaturation at temperatures slightly lower than aso-nAChR, and the cooperativity of denaturation is reduced (11). These altered biophysical properties of PC-nAChR have been attributed to weakened interactions leading to an increased physical separation between the agonist-binding and transmembrane domains (11). Weakened interactions could account for the increased solvent exposure, the reduced cooperativity of unfolding, and the lack of coupling of binding and gating (Fig. S6).

Significantly, we detect little if any structural or biophysical difference between PC-GLIC and either aso-GLIC or EcoLip-GLIC (Figs. 2 and 3). The amide I band shapes of GLIC in all three membranes are similar suggesting a similar global secondary structure (see, however, below). There is no further shift in amide I component band intensity from 1655 cm^{-1} down to near 1645 cm^{-1} after prolonged exposure of PC-GLIC to ^2H_2O. There are no changes in the levels of peptide N-^{1}H/N-^{2}H exchange, as shown by the similar residual amide II band intensities, although both aso-GLIC and PC-GLIC are more exchanged than EcoLip-GLIC. The thermal denaturation temperature of PC-GLIC is also similar to that of both aso-GLIC and EcoLip-GLIC and there are no changes in the cooperativity of unfolding (Table 1).

In fact, the only substantial difference observed between spectra recorded from PC-GLIC and either aso-GLIC or EcoLip-GLIC is a slight broadening of the amide I contour, noticeable near 1630 cm^{-1}. The degree of this

subtle broadening, however, varied between PC-GLIC purifications and reconstitutions. Although the structural basis of this spectral effect remains to be determined, it could reflect variations in GLIC aggregation within the membrane. Previous studies have suggested that the monodispersity of the pentameric GLIC within the membrane is lipid sensitive (18). Monodispersity was found to be ideal in asolectin bilayers. GLIC may tend to aggregate more in PC than in other lipid environments leading to broadening of the amide I band. Regardless, our structural data suggest that GLIC does not adopt an uncoupled conformation in PC membranes similar to that adopted by PC-nAChR.

Finally, we indirectly assessed whether PC-GLIC exhibits the ability to gate open in response to proton binding (Fig. 4). As noted, very weak or negligible Carb-induced current are observed in oocytes injected with PC-nAChR even though PC-nAChR fuses with the oocyte plasma membrane. In contrast, oocytes injected with PC-GLIC exhibit currents that both respond to protons in a dose-dependent manner and that are sensitive to amantadine block. The maximal currents obtained upon injection of PC-GLIC are substantially higher than those in mock or uninjected oocytes, and are indistinguishable from those observed in oocytes injected with either aso-GLIC or EcoLip-GLIC. The pH activated currents are also sensitive to amantadine. The electrophysiological recordings suggest that GLIC does not adopt a conformation in PC membranes similar to the uncoupled conformation adopted by the nAChR. Even the minimal PC membrane environment appears sufficient to stabilize GLIC in a conformation that gates open in response to agonist binding.

DISCUSSION

The underlying mechanisms by which lipids modulate nAChR function have been the subject of continuous debate for over 30 years (6). There has long been a consensus that both cholesterol and anionic lipids are required in a reconstituted membrane to obtain optimal nAChR function (7-10,34-36). It has also been suggested that both lipids influence nAChR function by an allosteric mechanism, whereby lipids alter the functional response to acetylcholine by stabilizing differing proportions of pre-existing resting (activatable) versus desensitized or uncoupled (inactivatable) conformations (7,29). The mechanisms by which these lipids influence function, however, are not clear. It has been suggested that some act by binding to interstitial sites between different α-helices in the transmembrane domain (13,37). Lipids may also interact directly with the lipid-protein interface (11,37-39). While the consensus is that lipid chemistry and thus specific lipid sites are likely important, both molecular details and direct experimental evidence for any mechanism of lipid action has yet to be obtained. The lack of mechanistic insight reflects both the complexity of lipid-nAChR interactions and the inability to express site directed mutants of the nAChR, which can be used to test proposed mechanisms of lipid-protein interactions.

Prokaryotic pLGICs provide a new opportunity for probing the molecular details of pLGIC-lipid interactions (14,40). The prokaryotic pLGIC, GLIC, adopts a similar tertiary fold to that of the nAChR. Both GLIC and the nAChR are cation-selective ion channels, although GLIC is gated by protons while the nAChR is gated by acetylcholine. The structural similarities of GLIC and the nAChR, as well as the added advantage that GLIC can be expressed in sufficient studies for biophysical and crystallographic studies has led the increasing use of GLIC as a model for probing pLGIC structure (15-17), basic mechanisms of pLGIC activation (15-17), pLGIC-drug interactions (41,42), etc. The ability to express large quantities of site-directed mutants finally opens the door for detailed mechanistic studies lipid-GLIC interactions. Such studies, however, first require a detailed characterization of the effects of lipids on GLIC structure and function.

We report here a simple protocol for reconstituting the prokaryotic pLGIC, GLIC, into defined lipid membranes. Our protocol differs from the standard vesicle detergent-destabilization approach typically used to form high lipid-to-protein ratio membranes for electro-physiological studies (18). One advantage of our approach is the high efficiency

incorporation of GLIC into the model membranes (Fig. S1). It is thus easy to accurately adjust the lipid-to-protein ratio of the reconstituted membranes. In addition, this protocol can be used to form relatively low lipid-to-protein ratio proteoliposomes.

Our goal was to reconstitute GLIC into membranes at lipid-to-protein ratios of roughly 2:1 (wt:wt) as the resulting vesicles are ideal for structural studies, such as those used previously to characterize the uncoupled nAChR. These low lipid-to-protein ratio vesicles can be easily separated from both protein-free vesicles and low lipid-protein ratio protein aggregates (see Fig. S1). They are ideal for spectroscopic studies because the scattering of light from the membrane vesicles (per mol of reconstituted protein) is minimized and the spectral overlap between signals from lipid and protein is less of an issue. The higher density low lipid-to-protein ratio proteoliposomes are easier to pellet (particularly in higher density ^2H_2O buffers) and thus exchange into $^2H_20$. Low lipid-to-protein ratio vesicles are also ideal for structural studies using infrared *difference* spectroscopy, a technique that detects residue-specific changes in structure of the nAChR upon agonist-binding (27,43,44). Application of this approach to prokaryotic pLGICs would be particularly informative given the ability to express mutants and thus assign detected vibrational changes to specific amino acid side chains.

Membrane-reconstituted GLIC and the nAChR exhibit similar structural and biophysical properties. Both proteins exhibit a mixed α-helix/β-sheet secondary structure with both a substantial proportion of the polypeptide backbone exposed to aqueous solvent and a large proportion of α-helical peptides shielded from solvent and likely found in the transmembrane channel pore domain. GLIC exhibits a higher β-sheet content than the nAChR, as expected given that the predominantly β-sheet agonist binding domain in GLIC makes up a larger proportion of the total protein structure (see below). The membrane reconstituted GLIC also undergoes thermal denaturation, albeit at higher temperatures than the nAChR. These observations show that the reconstituted GLIC maintains the expected structural fold.

On the other hand, infrared spectroscopy detects a relatively intense vibration near 1645 cm^{-1} in spectra of the nAChR due to solvent exposed α-helix and/or loop/random secondary structures. This vibration could reflect primarily the solvent exposed α-helix and loop/random secondary structures found in the intracellular domain of the nAChR (Fig. 1). The lack of similar intensity in this region in spectra of GLIC is consistent with the lack of an intracellular domain in the GLIC crystal structure.

We used an indirect electrophysiological approach to probe the ability of the reconstituted GLIC to gate open in response to agonist binding. Injection of membrane-reconstituted GLIC into oocytes led to the appearance of proton activated currents across the oocyte plasma membrane. The oocyte membrane incorporated GLIC responds in a dose-dependent manner to protons and the resulting currents were blocked by the GLIC channel blocker, amantadine. Both our structural and electrophysiological studies thus suggest that the reconstituted GLIC adopts a native structure that gates open in response to agonist binding.

A major goal of this work was to compare the lipid sensitivies of both GLIC and the nAChR. In particular, the nAChR in complex natural lipid membranes, such as those composed of either soybean asolectin lipids or mixtures of defined lipids (PC plus cholesterol and anionic lipids), adopts an activatable resting conformation. In contrast, the nAChR in PC membranes lacking the two "activating lipids" adopts an uncoupled conformation that binds agonist with a resting-state like affinity, but does not typically undergo agonist-induced conformational transitions. We are interested in the uncoupled nAChR because of increasing anecdotal evidence hinting that functionally uncoupled nAChRs may play a role in nicotinic receptor physiology (12). A main goal of this work was to assess whether GLIC exhibits propensity similar to that of the nAChR to adopt an uncoupled conformation in PC bilayers.

Although our data show that GLIC activity is sensitive to lipids (see below), PC-GLIC does not exhibit the structural or

functional characteristic of the uncoupled conformation adopted by PC-nAChR. PC-GLIC does not exhibit the substantial increase in solvent accessibility of polypeptide backbone hydrogens, which has been attributed to weakened interactions between the agonist-binding and transmembrane domains. PC-GLIC does not exhibit the reduced cooperativity of thermal denaturation that is observed for PC-nAChR. Finally, unlike PC-nAChR which remains inactive even after fusion with oocyte plasma membranes, fusion of PC-GLIC leads to an active conformation. Although further studies are required to fully characterize the functional properties of GLIC in different membranes, it appears that PC-GLIC is not locked in an uncoupled conformation that is unresponsive to agonist binding.

The finding that GLIC does not exhibit the same propensity as the nAChR to adopt an uncoupled conformation can be interpreted in light of our working model of uncoupling. This model proposes that lipids influence the coupling of binding and gating via the M4 transmembrane α-helices (one per subunit)(11), which are exposed to the surrounding lipid bilayer and thus ideally situated to sense membrane physical and/or chemical properties (Fig. 1)(45). Each M4 α-helix extends beyond the bilayer to interact directly with the Cys-loop, a key structure at the interface between the agonist binding (ABD) and transmembrane (TMD) domains. By influencing the conformation of the M4 "lipid-sensor", lipids may modulate interactions between M4 and the Cys-loop (Fig. S6 (11)). Weakened M4/Cys-loop interactions could lead to a Cys-loop conformational change that ultimately reduces contact between the agonist binding and the transmembrane domains, and leads to the uncoupled state.

A dynamic equilibrium may exist between coupled and uncoupled conformations where M4 is bound tightly or tilted away from the Cys-loop, respectively (46,47). In fact, an equilibrium between M4 solvated by lipid and M4 bound tightly to the other transmembrane α-helices, M1+M3, has been demonstrated for the homologous Glycine receptor (48). Significantly, aromatic-aromatic interactions play a key role driving associations between M4 and M1+M3 thus stabilizing a folded structure. In the context of the M4 lipid-sensor model, aromatic-aromatic interactions could play a key role dictating the propensity of M4 to bind tightly to M1+M3 and to thus form a coupled conformation. Aromatic-aromatic interactions could play a role dictating the propensity of a pLGIC to adopt an uncoupled conformation in PC membranes.

In light of this hypothesis, we compared the aromatic-aromatic interactions that exist between M4 and M1+M3 in GLIC versus the nAChR (Fig. 5). Consistent with the above hypothesis, GLIC exhibits a plethora of aromatic-aromatic interactions between M4 and M1+M3, with clusters located in both the cytoplasmic and extracellular leaflets of the lipid bilayer. These aromatics could lead to a highly stable transmembrane domain that is resistant to the formation of an uncoupled conformation. In contrast, while the nAChR exhibits aromatic residues at the interface between M4 and M1+M3, there appear to be few if any direct interactions that could stabilize the nAChR in a coupled conformation where M4 binds tightly to M1+M3, although the lower resolution of the nAChR structure makes this interpretation less definitive. Although other features likely play important roles, the paucity of aromatic-aromatic interactions between M4 and M1+M3 in the nAChR may contribute to weaker M4/M1+M3 interactions and thus to the high propensity of this receptor to adopt an uncoupled conformation. The lack of aromatic-aromatic interactions may also contribute to the lower thermal stability of the nAChR relative to GLIC. Future studies should lead to definitive insight into the molecular basis of lipid sensitivity in pLGICs.

Finally, it is notable that although GLIC does not exhibit the same propensity to uncouple as the nAChR, it still appears to be sensitive to its membrane environment. The dose response of membrane reconstituted GLIC incorporated into oocyte membranes is shifted to higher proton concentrations suggesting a weaker ability of protons to gate open the channel pLGIC. A lower pH_{50} has also been observed in electrophysiology studies of GLIC reconstituted into asolectin membranes at high lipid-protein ratios. In fact, lipid effects may account for the

altered pH_{50}s observed for GLIC in different heterologous expression systems (49,50). Note that altered sensitivity to protons could reflect altered proton binding and/or altered coupling of binding to gating. Lipids may still influence the coupling of binding and gating in GLIC, albeit to a lessor extent than with the nAChR.

In addition, we detect both an increased thermal stability and a reduced level of peptide backbone N-^{1}H/N-^{2}H exchange after prolonged exposure to $^{2}H_2O$ of EcoLip-GLIC relative to both aso-GLIC and PC-GLIC. Both suggest a slightly more rigid structure in the membranes formed from *E. coli* polar lipid extracts. A more detailed characterization of the effects of membranes on GLIC structure should lead to further insight into the molecular coupling of pLGICs with their membrane environment.

REFERENCES

1. Sine, S. M., and Engel, A. G. (2006) Recent advances in Cys-loop receptor structure and function. *Nature* **440**, 448-455
2. Taly, A., Corringer, P. J., Guedin, D., Lestage, P., and Changeux, J. P. (2009) Nicotinic receptors: allosteric transitions and therapeutic targets in the nervous system. *Nat Rev Drug Discov* **8**, 733-750
3. Sine, S. M. (2012) End-plate acetylcholine receptor: structure, mechanism, pharmacology, and disease. *Physiol Rev* **92**, 1189-1234
4. Changeux, J. P. (2012) Conscious processing: implications for general anesthesia. *Curr Opin Anaesthesiol* **25**, 397-404
5. Baenziger, J. E., and Corringer, P. J. (2011) 3D structure and allosteric modulation of the transmembrane domain of pentameric ligand-gated ion channels. *Neuropharmacology* **60**, 116-125
6. Heidmann, T., Sobel, A., Popot, J. L., and Changeux, J. P. (1980) Reconstitution of a functional acetylcholine receptor. Conservation of the conformational and allosteric transitions and recovery of the permeability response; role of lipids. *Eur J Biochem* **110**, 35-55
7. Baenziger, J. E., Morris, M. L., Darsaut, T. E., and Ryan, S. E. (2000) Effect of membrane lipid composition on the conformational equilibria of the nicotinic acetylcholine receptor. *J Biol Chem* **275**, 777-784
8. Hamouda, A. K., Sanghvi, M., Sauls, D., Machu, T. K., and Blanton, M. P. (2006) Assessing the lipid requirements of the Torpedo californica nicotinic acetylcholine receptor. *Biochemistry* **45**, 4327-4337
9. Fong, T. M., and McNamee, M. G. (1986) Correlation between acetylcholine receptor function and structural properties of membranes. *Biochemistry* **25**, 830-840.
10. Criado, M., Eibl, H., and Barrantes, F. J. (1982) Effects of lipids on acetylcholine receptor. Essential need of cholesterol for maintenance of agonist-induced state transitions in lipid vesicles. *Biochemistry* **21**, 3622-3629
11. daCosta, C. J., and Baenziger, J. E. (2009) A lipid-dependent uncoupled conformation of the acetylcholine receptor. *J Biol Chem* **284**, 17819-17825
12. Baenziger, J. E., and daCosta, C. J. B. (2012) Molecular mechanisms of acetylcholine receptor-lipid interactions: from model membranes to human biology. *Biophysical Reviews DOI: DOI 10.1007/s12551-012-0078-7*
13. Brannigan, G., Henin, J., Law, R., Eckenhoff, R., and Klein, M. L. (2008) Embedded cholesterol in the nicotinic acetylcholine receptor. *Proc Natl Acad Sci U S A* **105**, 14418-14423
14. Bocquet, N., Prado de Carvalho, L., Cartaud, J., Neyton, J., Le Poupon, C., Taly, A., Grutter, T., Changeux, J. P., and Corringer, P. J. (2007) A prokaryotic proton-gated ion channel from the nicotinic acetylcholine receptor family. *Nature* **445**, 116-119
15. Hilf, R. J., and Dutzler, R. (2008) X-ray structure of a prokaryotic pentameric ligand-gated ion channel. *Nature* **452**, 375-379
16. Bocquet, N., Nury, H., Baaden, M., Le Poupon, C., Changeux, J. P., Delarue, M., and Corringer, P. J. (2009) X-ray structure of a pentameric ligand-gated ion channel in an apparently open conformation. *Nature* **457**, 111-114
17. Hilf, R. J., and Dutzler, R. (2009) Structure of a potentially open state of a proton-activated pentameric ligand-gated ion channel. *Nature* **457**, 115-118
18. Velisetty, P., Chalamalasetti, S. V., and Chakrapani, S. (2012) Conformational transitions underlying pore opening and desensitization in membrane-embedded GLIC. *J Biol Chem*
19. Carswell, C. L., Rigden, M. D., and Baenziger, J. E. (2008) Expression, purification, and structural characterization of CfrA, a putative iron transporter from Campylobacter jejuni. *J Bacteriol* **190**, 5650-5662

20. Sayeed, W. M., and Baenziger, J. E. (2009) Structural characterization of the osmosensor ProP. *Biochim Biophys Acta* **1788**, 1108-1115
21. Hamouda, A. K., Chiara, D. C., Sauls, D., Cohen, J. B., and Blanton, M. P. (2006) Cholesterol Interacts with Transmembrane alpha-Helices M1, M3, and M4 of the Torpedo Nicotinic Acetylcholine Receptor: Photolabeling Studies Using [(3)H]Azicholesterol. *Biochemistry* **45**, 976-986
22. Reid, S. E., Moffat, D. J., and Baenziger, J. E. (1996) The selective enhancement and subsequent subtraction of atmospheric water vapour contributions from Fourier transform infrared spectra of proteins. *Spectrochimica Acta, Part A* **52**, 1347-1356
23. Pandhare, A., Hamouda, A. K., Staggs, B., Aggarwal, S., Duddempudi, P. K., Lever, J. R., Lapinsky, D. J., Jansen, M., Cohen, J. B., and Blanton, M. P. (2012) Bupropion binds to two sites in the Torpedo nicotinic acetylcholine receptor transmembrane domain: a photoaffinity labeling study with the bupropion analogue [(125)I]-SADU-3-72. *Biochemistry* **51**, 2425-2435
24. daCosta, C. J., and Baenziger, J. E. (2003) A rapid method for assessing lipid:protein and detergent:protein ratios in membrane-protein crystallization. *Acta Crystallogr D Biol Crystallogr* **59**, 77-83
25. Methot, N., Ritchie, B. D., Blanton, M. P., and Baenziger, J. E. (2001) Structure of the pore-forming transmembrane domain of a ligand-gated ion channel. *J Biol Chem* **276**, 23726-23732
26. Baenziger, J. E., and Chew, J. P. (1997) Desensitization of the nicotinic acetylcholine receptor mainly involves a structural change in solvent-accessible regions of the polypeptide backbone. *Biochemistry* **36**, 3617-3624
27. daCosta, C. J., Michel Sturgeon, R., Hamouda, A. K., Blanton, M. P., and Baenziger, J. E. (2011) Structural characterization and agonist binding to human alpha4beta2 nicotinic receptors. *Biochem Biophys Res Commun* **407**, 456-460
28. Baenziger, J. E., and Methot, N. (1995) Fourier transform infrared and hydrogen/deuterium exchange reveal an exchange-resistant core of alpha-helical peptide hydrogens in the nicotinic acetylcholine receptor. *J Biol Chem* **270**, 29129-29137
29. daCosta, C. J., Medaglia, S. A., Lavigne, N., Wang, S., Carswell, C. L., and Baenziger, J. E. (2009) Anionic lipids allosterically modulate multiple nicotinic acetylcholine receptor conformational equilibria. *J Biol Chem* **284**, 33841-33849
30. Unwin, N., and Fujiyoshi, Y. (2012) Gating movement of acetylcholine receptor caught by plunge-freezing. *J Mol Biol* **422**, 617-634
31. Alexandrov, A. I., Mileni, M., Chien, E. Y., Hanson, M. A., and Stevens, R. C. (2008) Microscale fluorescent thermal stability assay for membrane proteins. *Structure* **16**, 351-359
32. Morales, A., Aleu, J., Ivorra, I., Ferragut, J. A., Gonzalez-Ros, J. M., and Miledi, R. (1995) Incorporation of reconstituted acetylcholine receptors from Torpedo into the Xenopus oocyte membrane. *Proc Natl Acad Sci U S A* **92**, 8468-8472
33. Methot, N., Demers, C. N., and Baenziger, J. E. (1995) Structure of both the ligand- and lipid-dependent channel-inactive states of the nicotinic acetylcholine receptor probed by FTIR spectroscopy and hydrogen exchange. *Biochemistry* **34**, 15142-15149
34. Criado, M., Eibl, H., and Barrantes, F. J. (1984) Functional properties of the acetylcholine receptor incorporated in model lipid membranes. Differential effects of chain length and head group of phospholipids on receptor affinity states and receptor-mediated ion translocation. *J Biol Chem* **259**, 9188-9198
35. Rankin, S. E., Addona, G. H., Kloczewiak, M. A., Bugge, B., and Miller, K. W. (1997) The cholesterol dependence of activation and fast desensitization of the nicotinic acetylcholine receptor. *Biophys J* **73**, 2446-2455
36. Ryan, S. E., Demers, C. N., Chew, J. P., and Baenziger, J. E. (1996) Structural effects of neutral and anionic lipids on the nicotinic acetylcholine receptor. An infrared difference spectroscopy study. *J Biol Chem* **271**, 24590-24597

37. Jones, O. T., and McNamee, M. G. (1988) Annular and nonannular binding sites for cholesterol associated with the nicotinic acetylcholine receptor. *Biochemistry* **27**, 2364-2374
38. Marsh, D., Watts, A., and Barrantes, F. J. (1981) Phospholipid chain immobilization and steroid rotational immobilization in acetylcholine receptor-rich membranes from Torpedo marmorata. *Biochim Biophys Acta* **645**, 97-101
39. Ellena, J. F., Blazing, M. A., and McNamee, M. G. (1983) Lipid-protein interactions in reconstituted membranes containing acetylcholine receptor. *Biochemistry* **22**, 5523-5535
40. Tasneem, A., Iyer, L. M., Jakobsson, E., and Aravind, L. (2005) Identification of the prokaryotic ligand-gated ion channels and their implications for the mechanisms and origins of animal Cys-loop ion channels. *Genome Biol* **6**, R4
41. Nury, H., Van Renterghem, C., Weng, Y., Tran, A., Baaden, M., Dufresne, V., Changeux, J. P., Sonner, J. M., Delarue, M., and Corringer, P. J. (2011) X-ray structures of general anaesthetics bound to a pentameric ligand-gated ion channel. *Nature* **469**, 428-431
42. Weng, Y., Yang, L., Corringer, P. J., and Sonner, J. M. (2010) Anesthetic sensitivity of the Gloeobacter violaceus proton-gated ion channel. *Anesth Analg* **110**, 59-63
43. Ryan, S. E., Hill, D. G., and Baenziger, J. E. (2002) Dissecting the chemistry of nicotinic receptor-ligand interactions with infrared difference spectroscopy. *J Biol Chem* **277**, 10420-10426
44. Baenziger, J. E., Ryan, S. E., Goodreid, M. M., Vuong, N. Q., Sturgeon, R. M., and daCosta, C. J. (2008) Lipid composition alters drug action at the nicotinic acetylcholine receptor. *Mol Pharmacol* **73**, 880-890
45. Unwin, N. (2005) Refined structure of the nicotinic acetylcholine receptor at 4A resolution. *J Mol Biol* **346**, 967-989
46. de Almeida, R. F., Loura, L. M., Prieto, M., Watts, A., Fedorov, A., and Barrantes, F. J. (2006) Structure and dynamics of the gammaM4 transmembrane domain of the acetylcholine receptor in lipid bilayers: insights into receptor assembly and function. *Mol Membr Biol* **23**, 305-315
47. Xu, Y., Barrantes, F. J., Luo, X., Chen, K., Shen, J., and Jiang, H. (2005) Conformational dynamics of the nicotinic acetylcholine receptor channel: a 35-ns molecular dynamics simulation study. *J Am Chem Soc* **127**, 1291-1299
48. Haeger, S., Kuzmin, D., Detro-Dassen, S., Lang, N., Kilb, M., Tsetlin, V., Betz, H., Laube, B., and Schmalzing, G. (2010) An intramembrane aromatic network determines pentameric assembly of Cys-loop receptors. *Nat Struct Mol Biol* **17**, 90-98
49. Wang, H. L., Cheng, X., and Sine, S. M. (2011) Intra-membrane proton binding site linked to activation of a bacterial pentameric ion channel. *J Biol Chem*
50. Goyal, R., Salahudeen, A. A., and Jansen, M. (2011) Engineering a prokaryotic Cys-loop receptor with a third functional domain. *J Biol Chem* **286**, 34635-34642
51. Velisetty, P., and Chakrapani, S. (2012) Desensitization Mechanism in Prokaryotic Ligand-gated Ion Channel. *J Biol Chem* **287**, 18467-18477

Acknowledgements-We thank Julian Surujbali and Peter Juranka for assistance with the electrophysiological measurements.

FOOTNOTES

*This work was supported by grants from the Canadian Institute of Health Research and the Natural Sciences and Engineering Research Council of Canada to JEB, by a bourses d'études pour la France to JEB from l'Ambassade de France au Canada, and by grants from the South Plains Foundation and the Center for Membrane Protein Research, TTUHSC to M.P.B. and M.J. and by a grant from the National Institutes of Health Grant NS059841 to M.J.

[1]To whom correspondence should be addressed: John E. Baenziger, Department of Biochemistry, Microbiology, and Immunology, University of Ottawa, 451 Smyth Rd. Ottawa, ON, K1H 8M5, Canada, Tel.: (613) 562-5800 x8222; Fax.: (613) 562-5440; E-mail: John.Baenziger@uottawa.ca.
[2]Department of Pharmacology and Neuroscience and the Center for Membrane Protein Research, School of Medicine, Texas Tech University Health Sciences Center, Lubbock, TX 79430
[3]Department of Cell Physiology and Molecular Biophysics and the Center for Membrane Protein Research, School of Medicine, Texas Tech University Health Sciences Center, Lubbock, TX. 79430.
[4]G5 Group of Channel-Receptors, CNRS URA 2182, Pasteur Institute, F75015, Paris, France

[5]The abbreviations used are: aso-GLIC, GLIC in asolectin membranes; aso-naChR, nAChR in asolectin membranes; Carb, carbamylcholine; DDM, dodecylmaltoside; EcoLip-GLIC, GLIC in *E. coli* lipid membranes, GLIC, *Gloebacter* ligand-gated ion channel; nAChR, nicotinic acetylcholine receptor; pLGIC, pentameric ligand-gated ion channel; PC, 1-palmotyl-2-oleoyl-*sn*-glycero-3-phosphocholine; PC-GLIC, GLIC in PC membranes ; PC-nAChR, nAChR in PC membranes.

Table 1
Thermal stability of GLIC

Reconstitution	T_d	Hill Slope	*N*
aso-GLIC	68.8±1.5	2.44±0.16	5
EcoLip-GLIC	73.7±1.4	1.98±0.22	5
PC-GLIC	70.4±0.9	2.35±0.20	4
aso-nAChR	55.4±1.0	2.25±0.01	2
PC/PA/Chol-nAChR[a,b]	56.4±0.8	2.08±0.20	6
PC-nAChR[b]	52.4±0.1	3.08±0.12	6

[a]*the nAChR in membranes composed of PC, phosphatidic acid, and cholesterol*
[b]*from daCosta & Baenziger (11)*

FIGURE LEGENDS

Figure 1. The structures of (A) GLIC (pdb code 3EAM) and B) the *Torpedo* nAChR (pdb code 2BG9). Both structures are side views from within the plane of the membrane. Coloring highlights the domain structure: extracellular agonist-binding domain, red; transmembrane domain, purple; and cytoplasmic domain, green.

Figure 2. Structural comparisons of membrane-reconstituted GLIC and the nAChR as probed by infrared spectroscopy. (A) Infrared spectra of aso-GLIC recorded after gentle drying from $^{1}H_2O$ buffer (solid black line) and immediately after addition of $^{2}H_2O$ (dashed grey line). Note the immediate changes in amide I band shape (1700 – 1600 cm^{-1}) and the immediate decrease in amide II band intensity (1547 cm^{-1}), both indicative of the rapid peptide N-^{1}H/N-^{2}H exchange of solvent exposed peptide hydrogens. Similar spectral effects are observed for other Cys-loop receptors (Fig. S2). (B) Infrared spectra recorded after 72 hours equilibration in $^{2}H_2O$ at 4 ^{o}C from (i) aso-GLIC, (ii) EcoLip-GLIC, (iii) PC-GLIC, (iv) aso-nAChR, and (v) PC-nAChR. The left column shows the secondary structure sensitive amide I band both before (grey traces) and after resolution enhancement (black traces)(intensity scaling arbitrary). The right column shows the amide II band in each spectrum. The relative intensity of the amide II vibration is best assessed relative to the intensity of the adjacent broad peak between 1560 and 1600 cm^{-1}, due to aspartic and glutamic acid residues. All presented spectra are the average of several spectra recorded from at least two different purification/reconstitutions.

Figure 3. Representative thermal denaturation curves for GLIC (black lines) and the nAChR (grey lines) in different membranes. Denaturation curves are for aso-GLIC (▲), EcoLip-GLIC (●), PC-GLIC (□), aso-nAChR (△), PC/PA/Chol-nAChR (♦), and PC-nAChR (■). Each curve was fit with a Boltzmann sigmoid from which T_d and Boltzmann slope were calculated using GraphPad Prism software (Table 1)(see supplemental information of (11)). The Boltzmann slope decreases with increasing cooperativity of unfolding.

Figure 4. The Carb-induced response of membrane-reconstituted nAChR after injection into and consequent fusion with the plasma membrane of *Xenopus* oocytes. (A) Currents induced by 500 μM Carb were measured at -20 mV holding potential from oocytes injected with aso-nAChR (left trace) and PC-nAChR (right trace). (B) A bar graph comparing maximal recorded currents, each normalized to the number of [^{125}I]-α-Bungarotoxin (BTX) binding sites, induced by 300 μM acetylcholine from individual oocytes microinjected with 125 ng of affinity-purified *Torpedo* nAChR protein reconstituted in either PC/PA/CH (3:1:1 molar ratio; 0.124 ± 0.061 μA/[^{125}I]-α-Bungarotoxin binding sites/oocyte; n= 5) or PC lipid vesicles (0.0034 ± 0.0006 μA/[^{125}I]-α-Bungarotoxin binding sites/oocyte; *n*= 6).

Figure 5. The proton-induced response of membrane-reconstituted GLIC after injection into and consequent fusion with the plasma membrane of *Xenopus* oocytes. (A) Electrophysiology recordings in response to pH jumps from (i) uninjected oocytes and oocytes injected with (ii) aso-GLIC, (iii) EcoLip-GLIC, and (iv) PC-GLIC. The dose-response curves were measured at a relatively low membrane potential of -20 mV, as this seemed to generate more stable baselines. An electrical response to pH 4.0 showing the effect of 150μM amantadine (grey bar) is shown on the right (scaling arbitrary). The latter were performed at a membrane potential of -60 mV. (B) Peak current achieved upon exposure of oocytes injected with the indicated reconstituted membranes at pH 3.5. Reported values are the average±standard deviation from 5 recordings performed on 5 difference oocytes. (C) Comparison of the dose-response curves obtained from oocytes injected with the membrane-reconstituted GLIC or GLIC mRNA. The dose-response curves from oocytes injected with membrane-reconstituted GLIC were normalized assuming a pH_{50} of 2.90 according to Vilissetty *et al.*(51).

Figure 6. Aromatic-aromatic interactions may dictate the propensity of a pLGIC to adopt a lipid-dependent uncoupled conformation. Comparison of the aromatic residues located in M1, M3, and M4 of a single subunit transmembrane domain for (A) GLIC, and (B) the α-subunit of the nAChR. Both a side view of the transmembrane domain of each subunit and a top view looking down at the bilayer surface are shown. Note that the side view orientations of the two transmembrane domains has been rotated 180^{o} about the long axis of each molecule relative to the side view orientation shown in the schematic diagram of uncoupling in Fig. S7, as this presents a clearer view of the aromatic-aromatic interactions at the interface between M4 and M1+M3.

Figure 1

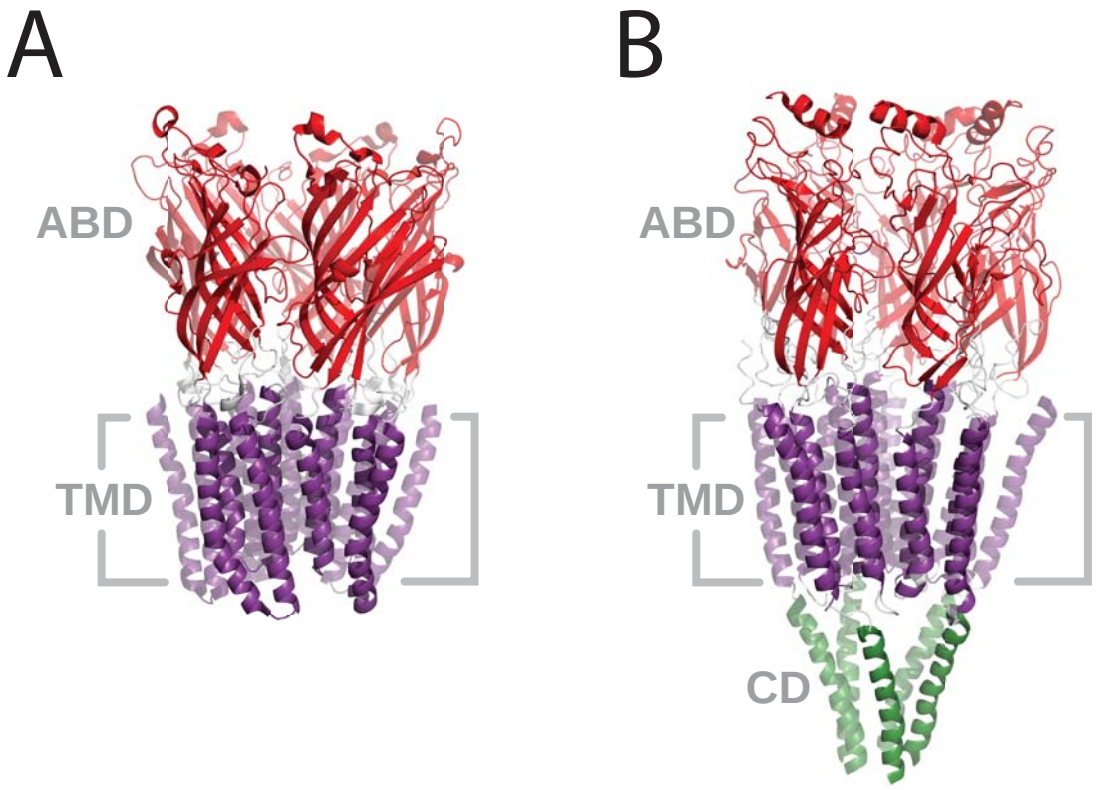

Figure 2

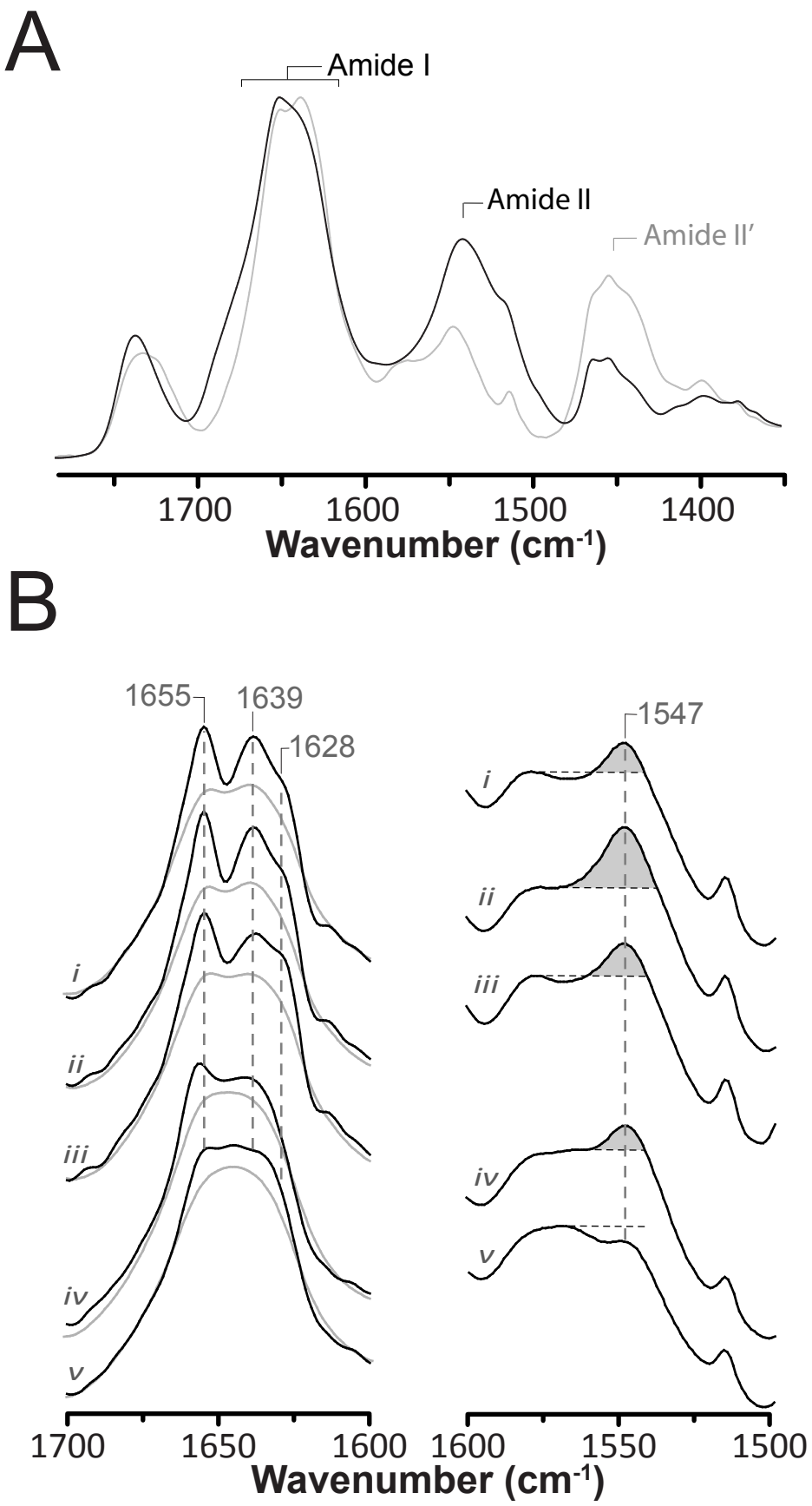

Figure 3

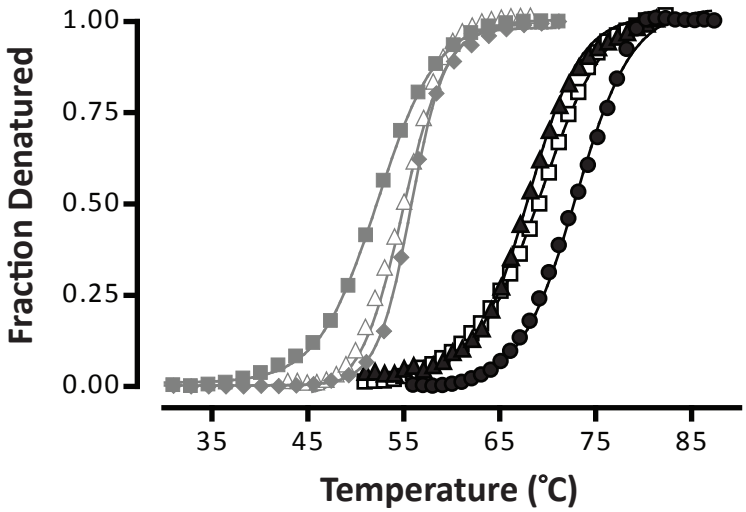

Figure 4

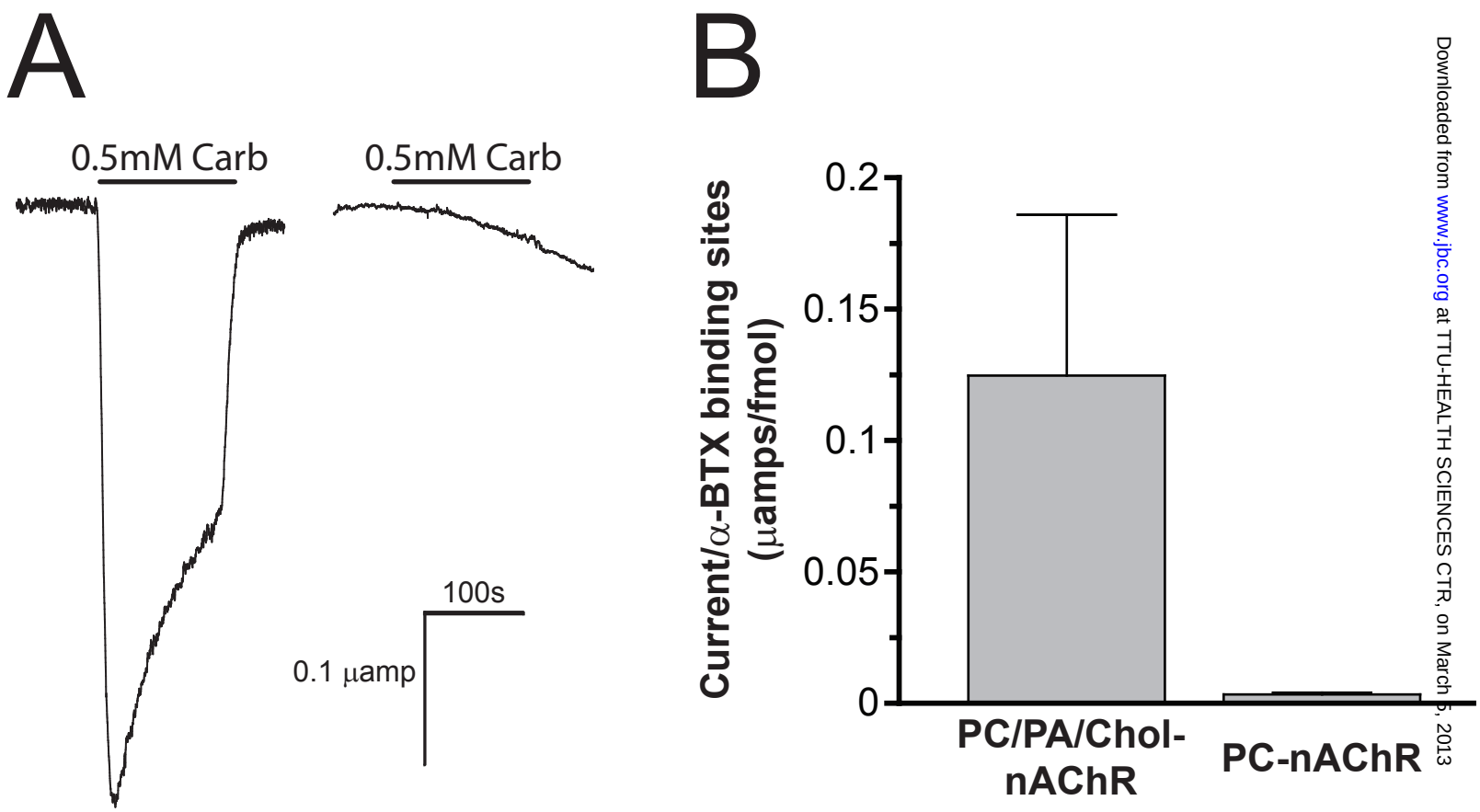

Figure 5

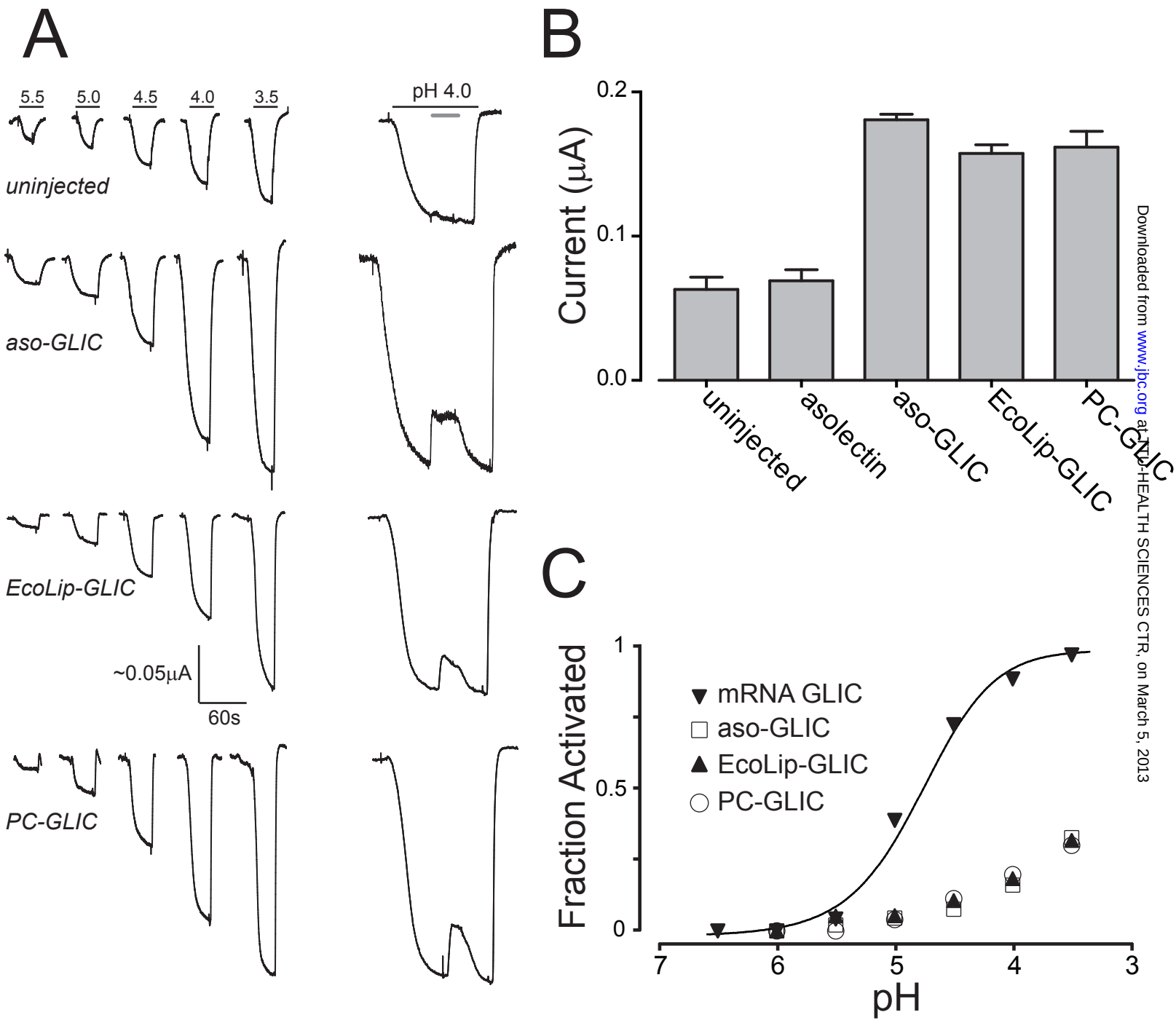

Figure 6

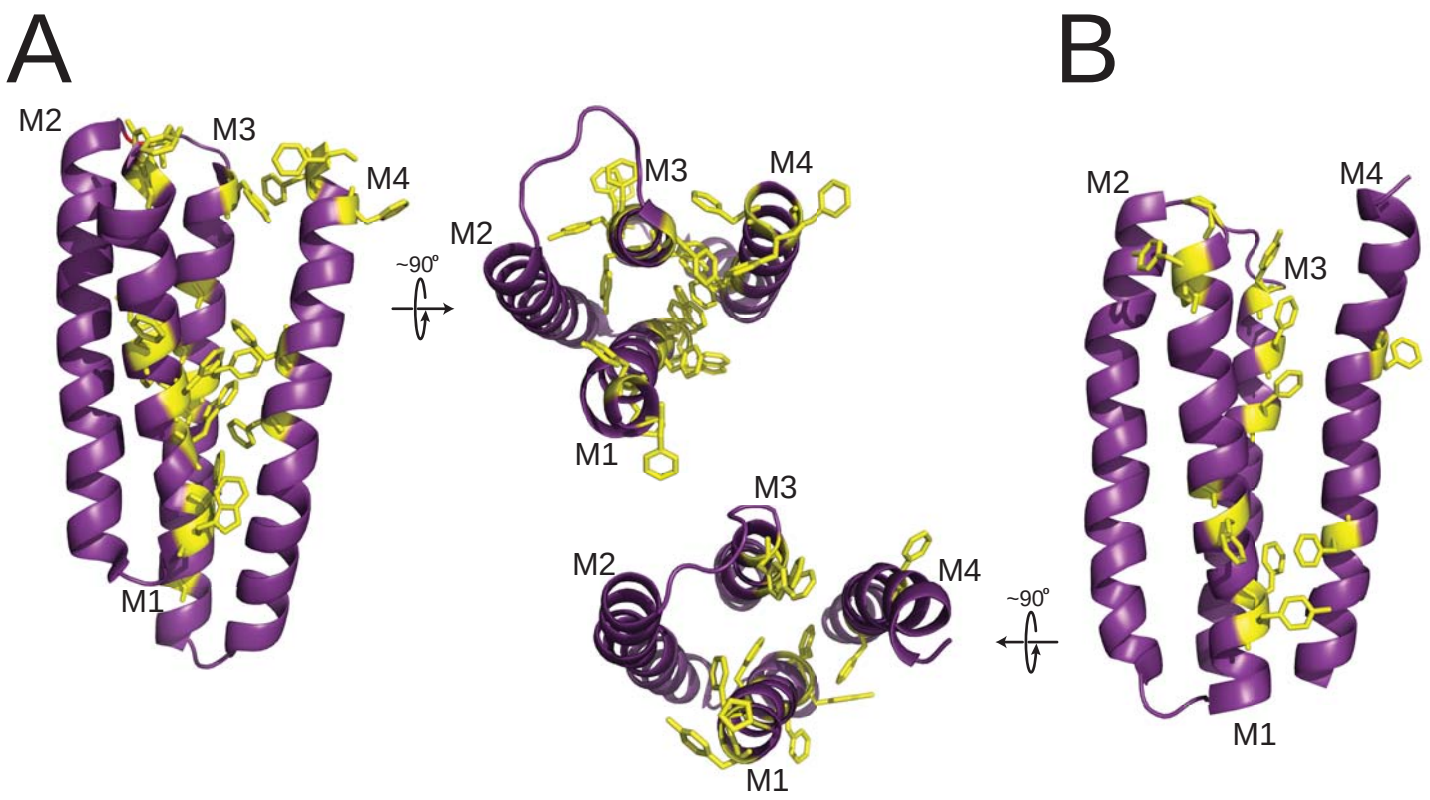

SUPPLEMENTARY MATERIAL for

Structural sensitivity of a prokaryotic pentameric ligand-gated ion channel to its membrane environment*

Jonathan M. Labriola[1], Akash Pandhare[2], Michaela Jansen[3], Michael P. Blanton[2], Pierre-Jean Corringer[4], and John E. Baenziger[1]

[1]From the Department of Biochemistry, Microbiology, and Immunology
University of Ottawa, Ottawa ON, K1H 8M5, Canada

[2]Department of Pharmacology and Neuroscience and the Center for Membrane Protein Research, School of Medicine, Texas Tech University Health Sciences Center, Lubbock, TX 79430

[3]Department of Cell Physiology and Molecular Biophysics and the Center for Membrane Protein Research, School of Medicine, Texas Tech University Health Sciences Center, Lubbock, TX. 79430.

[4]G5 Group of Channel-Receptors, CNRS URA 2182
Pasteur Institute, F75015, Paris, France

*Running title: *Lipid sensitivity of a prokaryotic pLGIC*

[1]To whom correspondence should be addressed: John E. Baenziger, Department of Biochemistry, Microbiology, and Immunology, University of Ottawa, 451 Smyth Rd. Ottawa, ON, K1H 8M5, Canada, Tel.: (613) 562-5800 x8222; Fax.: (613) 562-5440; E-mail: John.Baenziger@uottawa.ca.

Includes: Supplemental Figures S1-S6 with captions

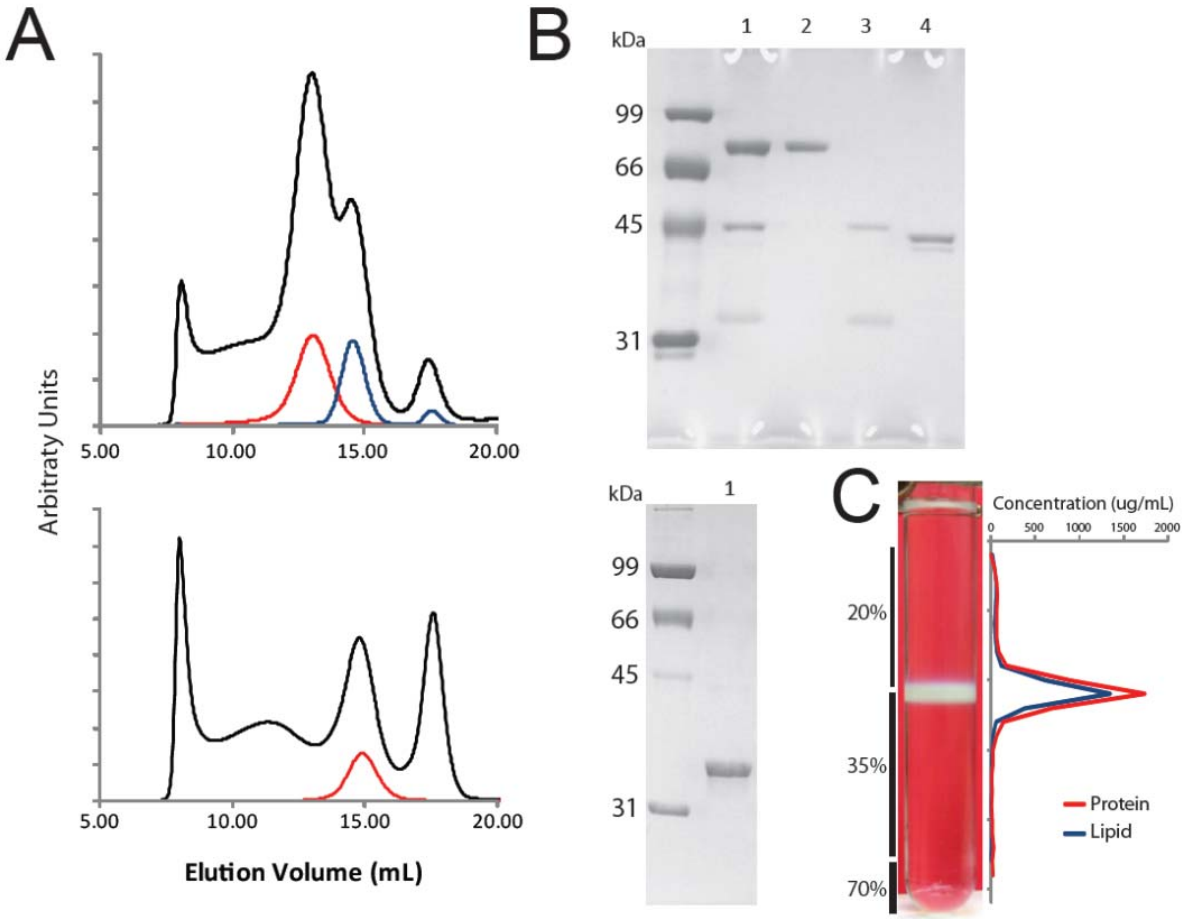

Figure S1. Purification and reconstitution of GLIC. (A) The elution profiles of MBP-GLIC (top set of traces) or GLIC (bottom traces) from an SEC column. In both cases, MBP-GLIC was affinity purified on an amylose affinity resin. The MBP-GLIC was eluted using maltose, while GLIC was eluted after cleavage of the MBP-GLIC linker with thrombin. The affinity purified proteins were concentrated and then passed through the SEC column leading to the elution profiles shown in black. In the top set of traces, the red trace ~13 mls corresponds to purified MBP-GLIC, the purple trace at ~15 mls corresponds to an endogenous *E. coli* protein that binds to the amylose resin, and the purple trace at ~17 mls corresponds to MBP. In the bottom set of traces, the red trace at ~15 mls corresponds to purified GLIC. Individual traces are arbitrarily scaled for presentation purposes. (B) SDS PAGE gels of the eluted fractions from the SEC. Top gel *Lane 1*, concentrated MBP-GLIC plus endogenous *E. coli* protein eluted from the amylose affinity resin; *Lane* 2, MBP-GLIC; *Lane 3*, unknown *E. coli* protein; *Lane 4*, MBP. Bottom gel *Lane 1*, purified GLIC. (C) Sucrose density gradient purification of reconstituted aso-GLIC showing complete incorporation of GLIC into the asolectin membranes. The lipid assay measures choline content, and thus underestimates the lipid content of the reconstituted membranes.

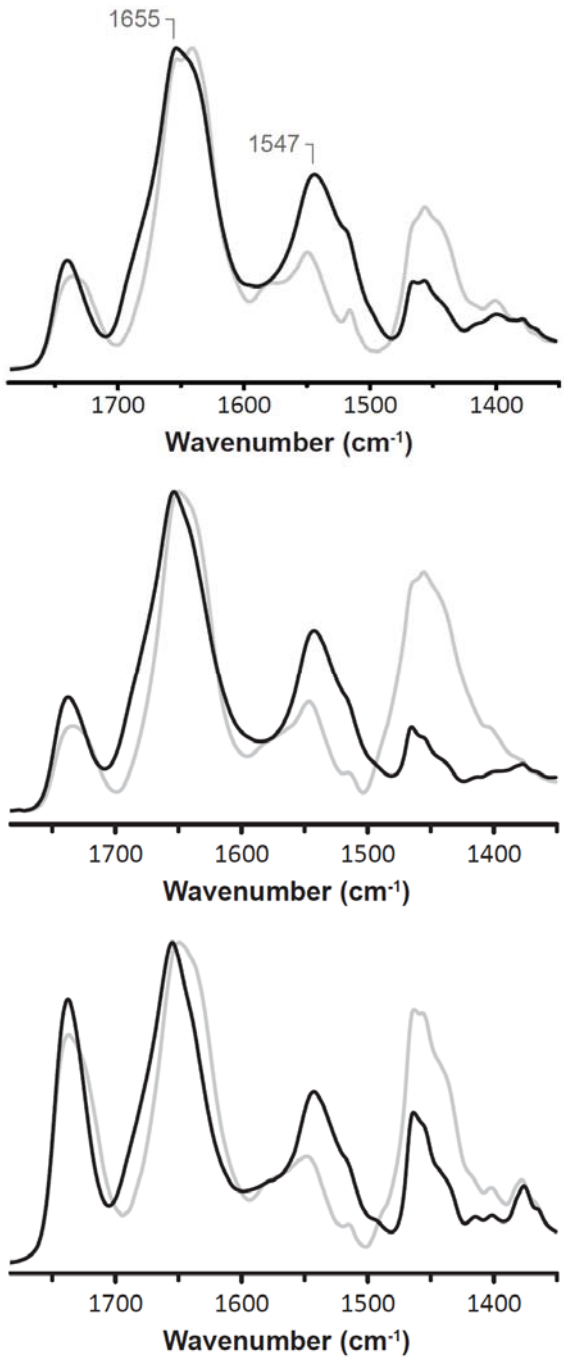

Figure S2. Infrared spectra recorded from (A) GLIC, (B) the nAChR, and (C) the α4β2 neuronal nAChR recorded after gentle drying to remove bulk solvent from $^{1}H_2O$ buffer (solid black line) and immediately after addition of $^{2}H_2O$ (dashed grey line). Note the immediate changes in amide I band shape (1700 – 1600 cm^{-1}) and the immediate decrease in amide II band intensity (1547 cm^{-1}), both indicative of the rapid peptide N-^{1}H/N-^{2}H exchange of solvent exposed regions of the polypeptide backbone. (data from daCosta et al. (2011) *Biochem Biophy. Res Commun* **407**, 456-460)

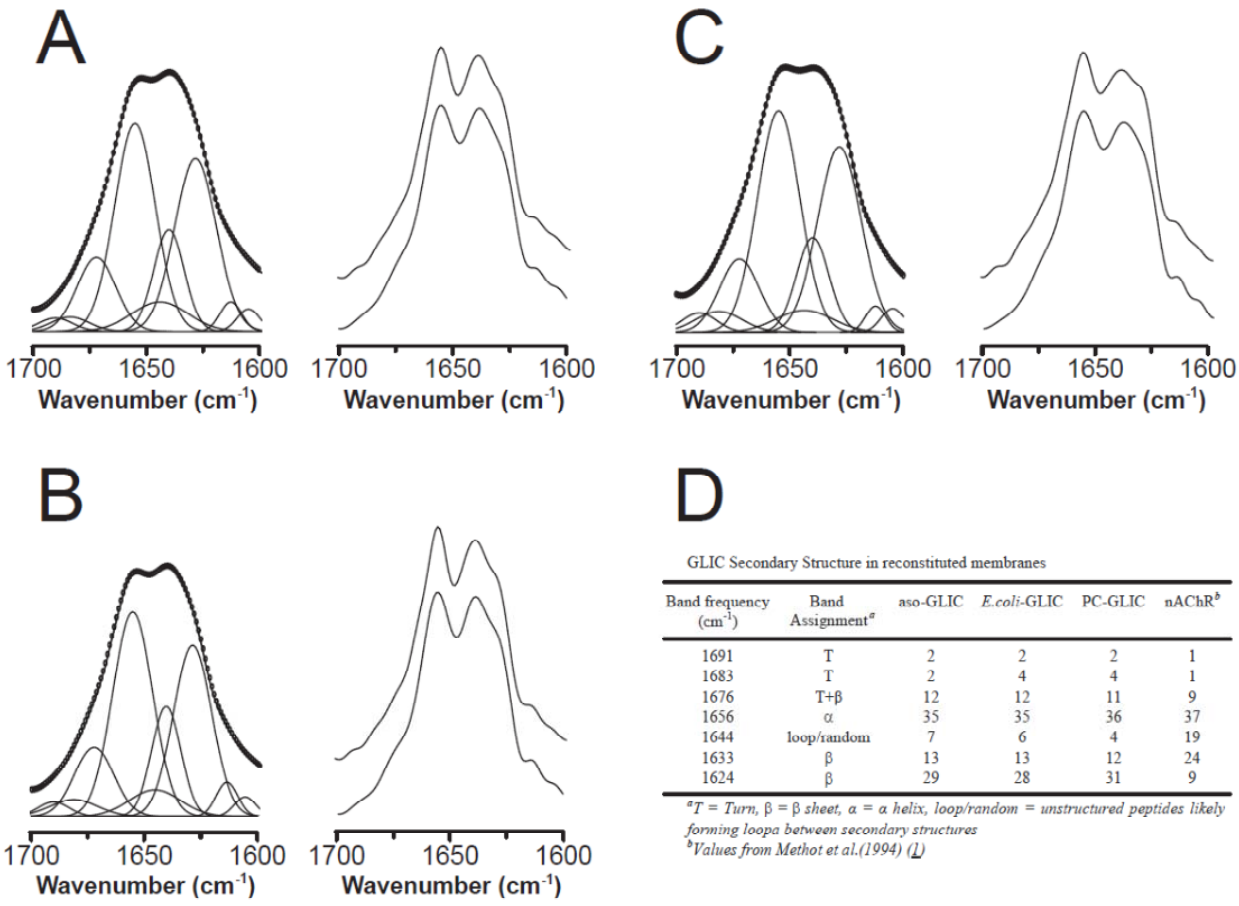

D

GLIC Secondary Structure in reconstituted membranes

Band frequency (cm^{-1})	Band Assignment[a]	aso-GLIC	*E.coli*-GLIC	PC-GLIC	nAChR[b]
1691	T	2	2	2	1
1683	T	2	4	4	1
1676	T+β	12	12	11	9
1656	α	35	35	36	37
1644	loop/random	7	6	4	19
1633	β	13	13	12	24
1624	β	29	28	31	9

[a] *T = Turn, β = β sheet, α = α helix, loop/random = unstructured peptides likely forming loops between secondary structures*

[b] *Values from Methot et al.(1994) (1)*

Figure S3. Representative curve fits of the amide I bands from (A) aso-GLIC, (B) EcoLip-GLIC, and (C) PC-GLIC. In each case, the left set of spectra include the experimental amide I absorbance contour (black line), the superimposed curve fit (open circles), and the individual component peaks summed to curve fit amide I contour. The two spectra on the right correspond to the the deconvolved experimental spectrum (top) and the deconvolved curve fit spectrum (bottom). (D) The resulting curve fit estimates and band assignments.

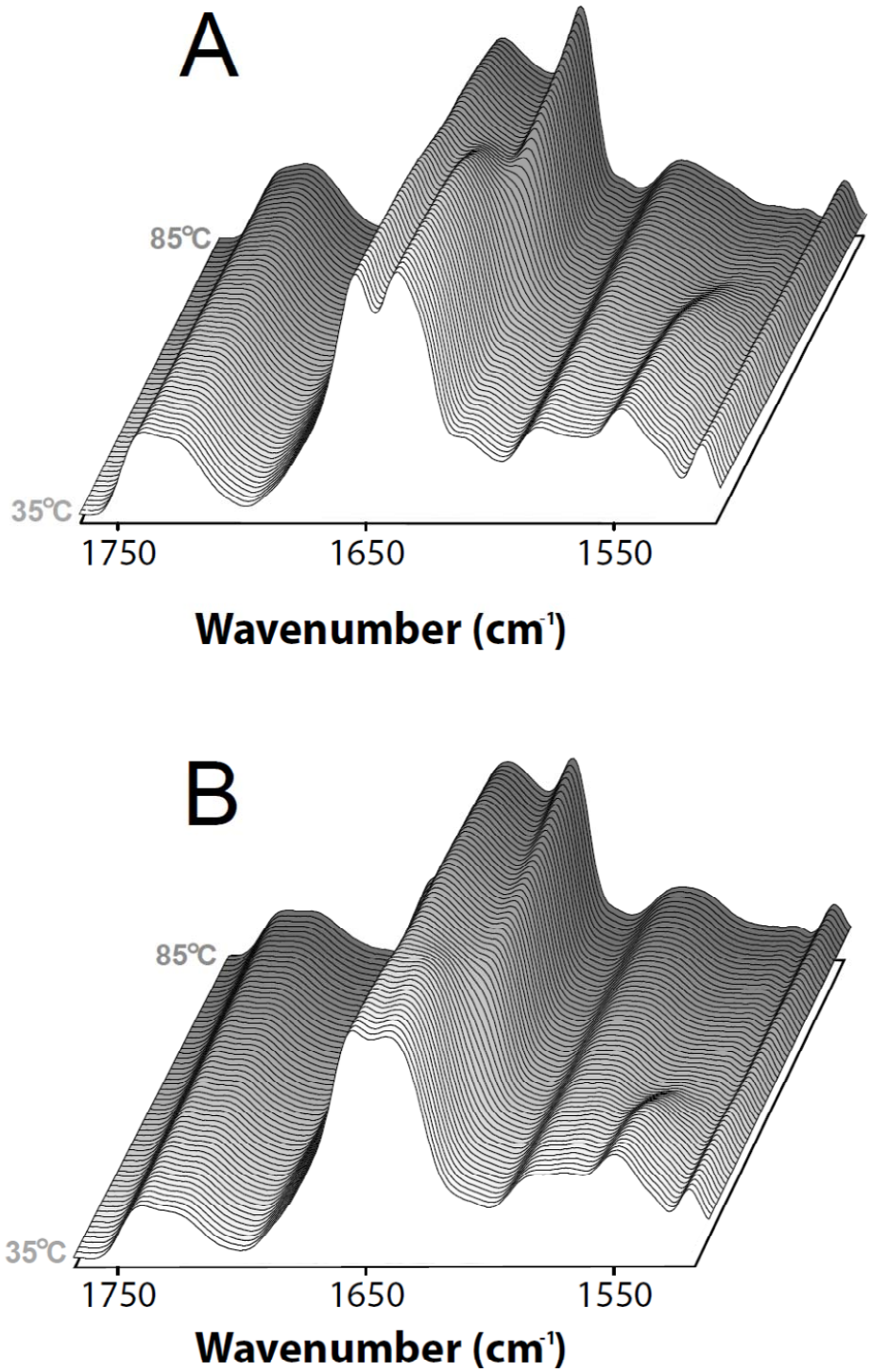

Figure S4. Stacked plot of spectra collected for thermal stability characterization of (A) aso-GLIC and (B) aso-nAChR. Representative traces are shown from 35 °C to 85 °C, front to back. Spectra were collected at 1˚C increments.

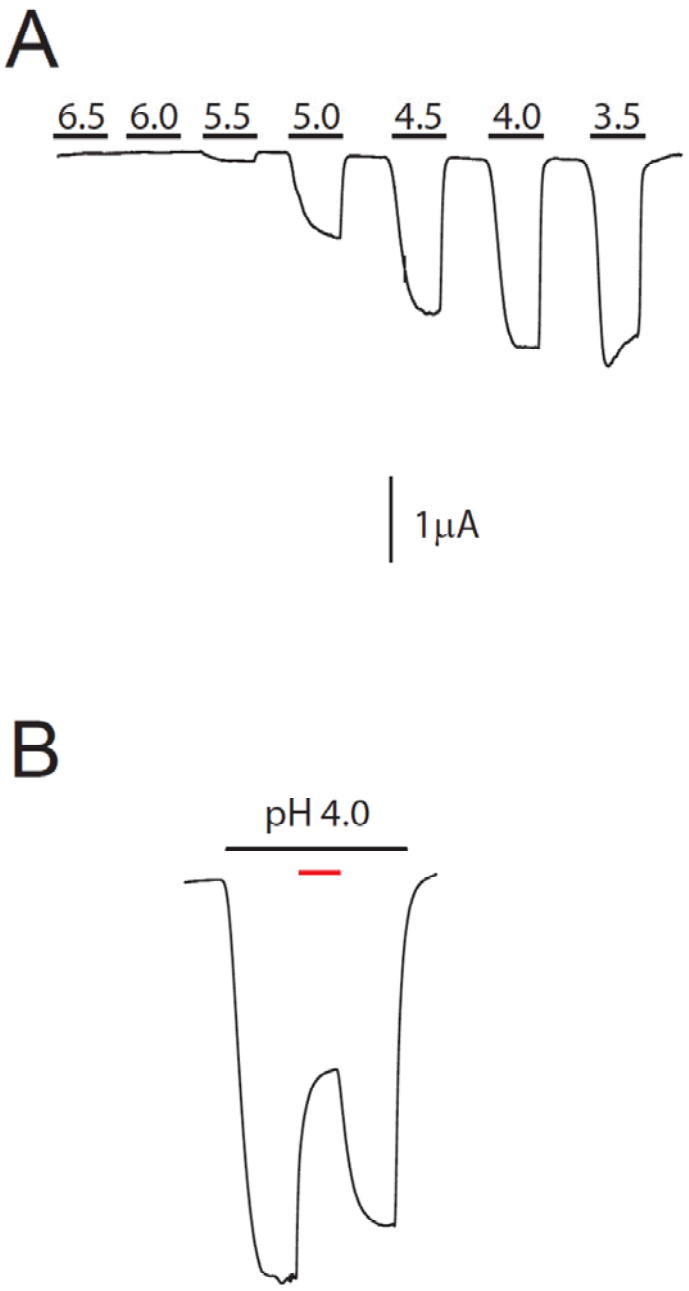

Figure S5. Current traces of mRNA-GLIC injected oocyted probed by two-electrode voltage clamp. (A) Currents induced by exposure to the pH jumps indicated by the horizontal bars. Cells were held at a membrane potential of -20 mV. (B) mRNA-GLIC injected oocytes were held at a membrane potential of -60mV and exposed to pH 4.0 until steady state was achieved, after which 150μM amantadine (pH 4.0) was introduced into cell profusion chamber (red bar) followed by washout.

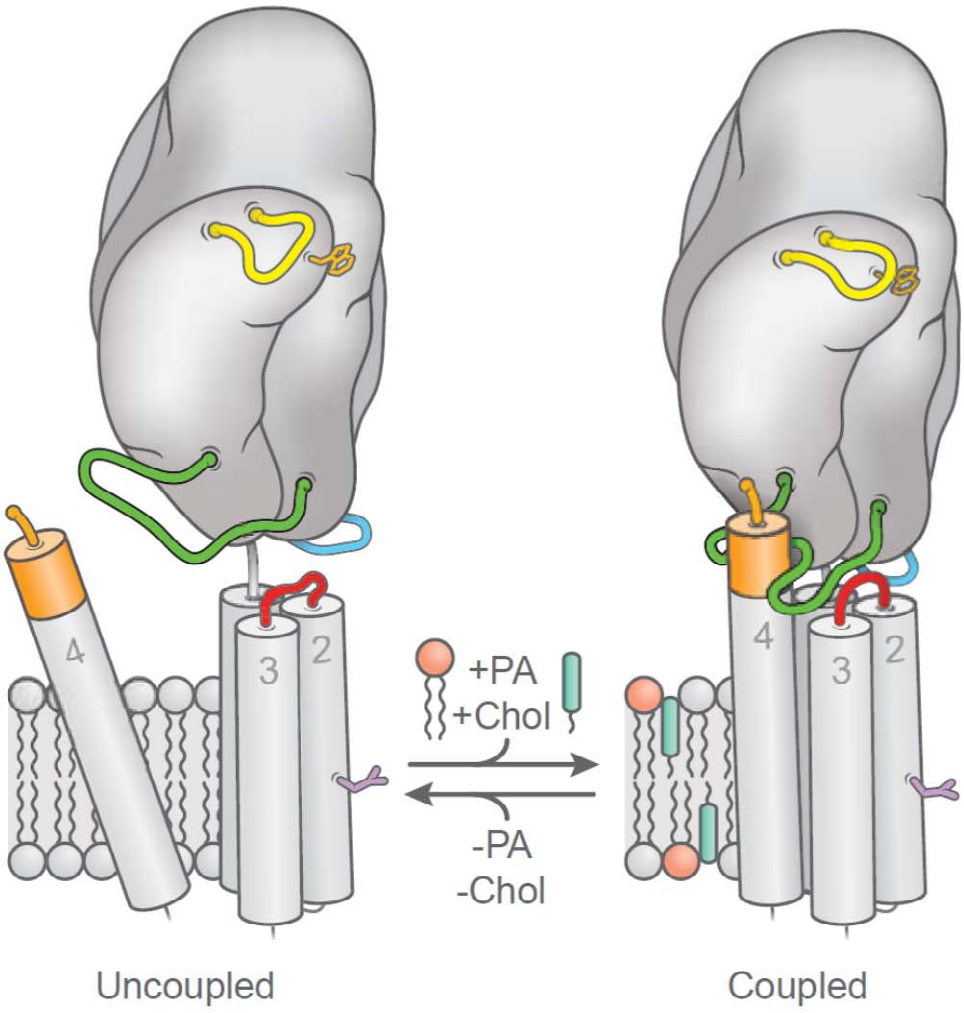

Figure S6. The M4 lipid-sensor model of uncoupling. The model proposes that interactions between the C-terminus of M4 (orange) forms critical interactions with the Cys-loop (green) of the agonist binding domain. When optimal interactions occur, the Cys-loop adopts a conformation that allows tight interactions with the M2-M3 linker. These tight interactions are essential for coupling binding to gating. In unfavorable lipid environments, the interactions between M4 and the Cys-loop are not optimatal. This leads to an altered conformation of the Cys-loop and weakened interactions between the Cys-loop and M2-M3 linker. Weakened interactions leads to a physical separation between the agonist-binding and transmembrane domains and thus the uncoupling of binding and gating. (daCosta & Baenziger (2009) *J Biol Chem* **284**, 17819-17825)